GEOLOGICAL MODELING AND SIMULATION OF CO_2 INJECTION IN THE JOHANSEN FORMATION

G. T. EIGESTAD, H. K. DAHLE, B. HELLEVANG, F. RIIS, W. T. JOHANSEN, AND E. ØIAN

ABSTRACT. The Johansen formation is candidate site for large scale CO_2 storage offshore the south-western coast of Norway. An overview of the geology for the Johansen formation and neighbouring geological formations is given, together with a discussion of issues for geological and geophysical modelling, and integrated fluid flow modelling. We further describe corresponding simulation models. Major issues to consider are capacity estimation and processes that could potentially cause CO_2 to leak out of the Johansen formation and into the formations above.

Currently, these issues can only be investigated through numerical simulation. We consider the effect of different boundary conditions, sensitivity with respect to vertical grid refinement and permeability/transmisibility data, and the effect of residual gas saturations since these strongly affect the CO_2-plume distribution. The geological study of the Johansen formation is performed based on available seismic and well data. Fluid simulations are performed using a commercial simulator capable of modelling CO_2 flow and transport by simple manipulation of input files and data. We provide details for the data and the model, with a particular focus on geology and geometry for the Johansen formation. The dataset is made available for download online.

1. INTRODUCTION

The importance of finding ways to deal with CO_2 emissions has initiated specific projects where the ultimate goal is to store large quantities of CO_2 in deep saline aquifers. The Norwegian government has promoted two gas power plants with full scale CO_2 handling (CCS) located at Kårstø and Mongstad at the south-western coast of Norway, see Figure 1. The Kårstø plant may produce 1.1 Mt CO_2/yr and should have full scale CCS by 2012, whereas the Mongstad plant will produce 2.2 Mt CO_2/yr and should be operational with full scale CCS by 2014 [9].

The Matched Storage Capacity [5], [7] that needs to be demonstrated for potential storage sites is therefore of the order of 4 Mt CO_2 /year. Two geological formations offshore Norway are currently investigated. The Utsira formation is well documented and considerable experience is already gained because 1 Mt CO_2/yr has been injected into this formation from the Sleipner gas field since 1996, [24]. Here we will focus on the second potential storage site: The Johansen formation is a deep saline aquifer located below the Troll-field, see Figure 1. It has large volumes, suited pressure regimes at the large depths, close well

access from the Troll field, promising geological properties and sealing properties shown by initial modeling, and proximity to Mongstad. The Johansen formation therefore appears to be an excellent candidate for storage of CO_2 from Kårstø and particularly the Mongstad power plant. Early case studies [9] have also shown pipeline solutions to outperform combined wessel/pipeline solutions in terms of economical viability, and a long term pipeline solution from Mongstad may be feasible.

The estimation of the storage capacity of deep saline aquifers is very complex since various trapping mechanisms are involved and act on different time scales [4],[5],[7],[15], [26]. Geological uncertainty and/or lack of geological characterization add further to this complexity. In the end, conservative estimates of the amount of CO_2 that escape the boundaries of an aquifer within a given time frame, and the consequences of leakage must be provided. Because of computational limitations and lack of information which require a stochastic framework, new modeling tools need to be developed to perform this type of analysis. Such modeling tools have been proposed and are developed by Celia and Nordbotten with collaborators in the context of mature sedimentary basins in the North America, see [18], [19], [20], [21], [22]. Their focuses have been to handle large numbers of abandoned and potentially leaky wells within simple layered geometry which allows for semi-analytic solutions. North Sea aquifers may on the on the other hand provide different challenges, including complex geometries and fault/fracture zones which may provide pathways for leakage. To understand the main effects that should be accounted for in capacity/risk analysis, detailed simulations must be performed using verified simulation tools as a first step.

The purpose of this work is two-folded: First we wish to provide a background to the benchmark 3 problem presented at the Workshop on Numerical Models for Carbon Dioxide Storage in Geological Formations, Stuttgart April 2-4, 2008, [8]. This was a benchmark study based on the geological data for the Johansen formation, but on a simplified geometry and a small extract of the entire model. The workshop demonstrated that different modeling groups need to communicate to calibrate and understand the workings of computational tools, but also the need for real data to be provided for the modeling community. The geological model presented in this work is therefore made available online, see [11], and a complete dataset is made available for simple CO_2 flow. Secondly, we investigate some of the factors that we believe are important in obtaining reliable capacity estimates of a formation, using the commercial simulator Eclipse 100 [12]. The numerical simulations presented here may be used for comparisons of simulations, and a motivation for more advanced studies. Probably one of the most important factors is to determine appropriate boundary conditions for the formation. We show that different choices of boundary conditions strongly affect the time variation of the pressure field and the CO_2 plume distribution. A major numerical concern is the need for grid resolution. We show that a fairly fine vertical resolution is needed to capture the CO_2 plume that follows the sealed roof of the formation due to gravity override. Moreover, vertical grid refinement of the sealing shale layer is needed because of upstream weighting in the numerical simulation tool. The upstream weighting without grid refinement

leads to numerical diffusion which may appear as leakage into the formations above. Consequently, the numerical resolution may need to be higher than in the original geological grid. We then simulate post injection migration to investigate the potential effect of residual trapping and relative permeability models. The geometry and topology of the geological medium will also play a key part for CO_2 distribution. Finally, we investigate the sensitivity of the plume distribution with respect to permeability models. Dissolution and mineral trapping mechanisms [4],[5] are not considered in this work and are typically important over longer time-scales than the simulation studies performed here.

The rest of the paper is organised as follows: Section 2 provides an overview, and discusses geological modeling of the formation. Section 3 gives more details of the data which is made available, and discusses simulation issues and set-up. Section 4 presents some simulation results for injection of CO_2 in the Johansen formation. Conclusions are given in Section 5.

2. Overview of the Johansen formation and geological modeling

The Johansen formation is located in the deeper part of the Sognefjord delta, 60 km offshore the Mongstad area at the west coast of Norway. The Troll field is situated some 500 meters above the north-western parts of the Johansen formation, and is one of the largest gas fields in the North Sea. The Sognefjord Formation which is situated more than 500 meters above the Johansen Formation, is the uppermost sand in the Sognefjord delta. The Sognefjord Formation is the main reservoir for the giant Troll gas and oil field. Figure 1 shows the geographic locations of various fields and sites of interest together with parts of the south-western coast of Norway. The two red dots indicate the location the planned power plants at Kårstø and Mongstad. The depth levels of the Johansen formation range from 2200-3100 m below sea level, which makes the formation ideal for CO_2 storage due to the pressure regimes that exist here. The average thickness of the formation is roughly 100 m and the lateral extensions are up to 100 km in the north-south direction and 60 km in the east-west direction. With average porosities of approximately 25 percent this implies that the theoretical storage capacity of the Johansen formation is of the order > 1 Gt CO_2 when also accounting for residual brine saturation (approximately 20 percent).

Figure 2 shows a cross-section from the geological model in the southern part of the proposed injection area. Mainly sandy layers are shown by yellow colours, and shaly layers with grey and black. The Troll Field is located above 1550 m depth north and east of the section (red colour). The model is based on mapping of the existing seismic and well data, including high quality 3D seismic data sets in the area of the Troll Field, and a 2D seismic grid of fair quality from the 1990'ies south of the field. We have used log data from 12 exploration wells in the Troll Field and a few additional wells from neighbouring fields which have penetrated the Johansen Formation or its equivalents. One of the wells has a short core in the Johansen Formation. The purpose of the model was to serve as a basis for a quick evaluation of the feasibility of using the Johansen formation for CO2 sequestration. Consequently, the model represents a simplification of
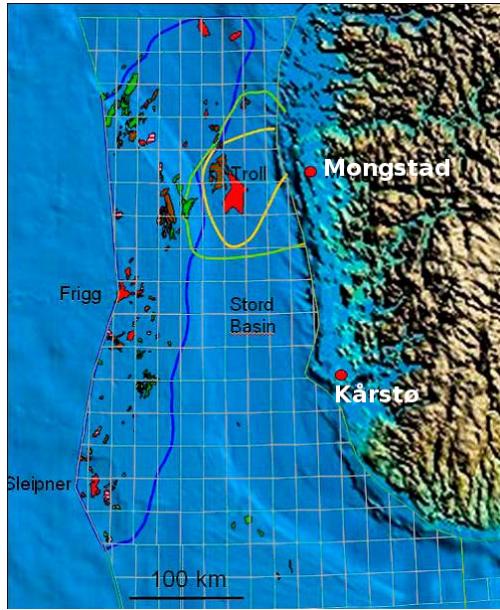
FIGURE 1. Schematic of locations of the Utsira and Johansen formations. The Johansen formation is contained within the green curve, and the yellow curve represents areas where seismics is known. The Norwegian sector of the Utsira formation is bounded by the blue line (Courtesy of Gassnova).

the geological layering, and in particular the Dunlin Group (black), although predominantly shaly, can be subdivided in different formations, some of which are locally sandy. The Johansen Formation itself has been divided into three zones, which have been extended all over the area. This is also a simplification of the geology, as it is likely that the formation in reality consists of several sand bodies with less lateral continuity. The general delta front depositional environment suggests, however, that there will be good communication between the sand bodies.

In Figure 2, the major fault surfaces are shown with grey shades. The fault interpretation is based on the seismic data. The fault throws and intensity is much smaller in the south than in the north. The most significant fault in the study area is the main north-south trending fault which can be seen to cause a small high in the central part of the cross-section, and which continues to the north to separate the western part of the Troll Field into two segments. Seismic data have also been used to model the area of pinching out of the Johansen Formation to the west. The pinch-out is confirmed by well data in the Brage Field west of the modelled area. Porosity and permeability values in the model are based on the log and core data from the exploration wells. The porosities in the model are calculated for each layer in the Johansen Formation by using a porosity-depth trend for each of the zones. Additional well data from the Fram Field north of Troll were used to obtain reliable trends towards depth, since all Troll wells are shallow. The permeability values in the model are calculated
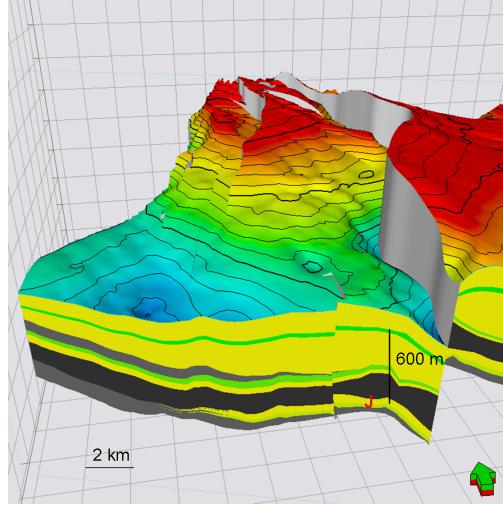
FIGURE 2. Geological model of area that is being investigated for CO_2 storage in the Johansen formation. Topographical surface shows top of sandstone reservoir where the Troll gas is located. Troll field indicated by red coloring. Cross section shows different layers downward in the formations. Dark coloring indicates shale, yellow layers are sandstone. The Johansen formation is approximately 600 m below the sandstone layers of Troll, and they are separated by several layers of shale.

from porosity-permeability trends obtained from comparable lithologies from the Sognefjord Formation due to the limited data from the Johansen Formation. It should be noted that the fairly localized well data may call for the need to drill a well in the proposed injection area for data analysis and geo-modelling. Particularly important issues for early assessment of the Johansen formation as a storage site for CO_2 are volume, injectivity and sealing properties. Geological modelling indicates that layers of shale and sandstone separate the Johansen formation from the formations above, and serve mainly as horizontal sealing. In particular, shales of the Dunlin Group lie immediately above the Johansen formation, and serve as a cap-rock for the formation. The Dunlin Group is mostly very thick, in certain areas up to hundreds of meters, but may vanish in some of the eastern areas of the formation. However, the planned injection site is far away from these areas. The thickness of the Dunlin Group is visualized in Figure 3. The Dunlin Group has high clay/silt content. The impact of this is that the faults incorporated in the model have a predominantly sealing effect. From a CO_2 storage point of view the combination of thick layers of shale and sealing faults, is appealing due to the volumes of static traps these may set up Possible leakage pathways for CO_2 may arise if shale vanishes or faults are not everywhere sealed. Currently, the geological model does not capture such issues in any detail. Further geological modelling may be done to assess the sealing quality of the faults due to smearing of the fault planes based on fault throw and clay content. The possibility that permeable lenses occur within the smeared fault zones may set up leakage paths to formations above. Leakage
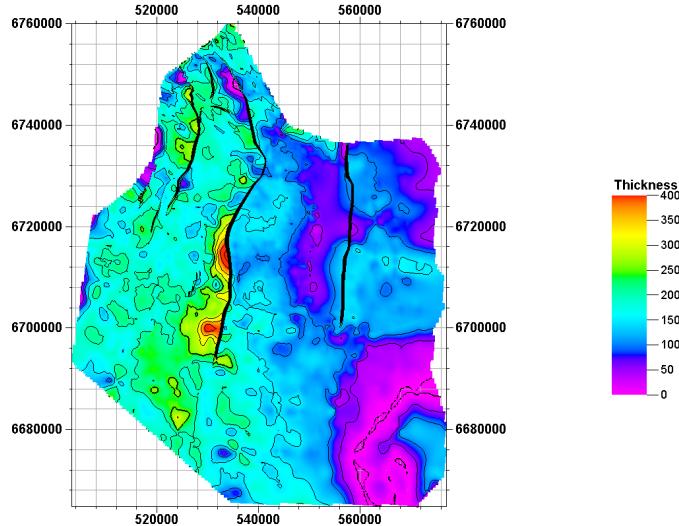
FIGURE 3. Varying thickness of Dunlin group above Johansen formation. Vanishing shale observed in the south-eastern parts of the area of the available geo-model. Notice the area with thick shale; this area is immediately to the west of the main fault in the model, which is seen as one of the thick, dark curves in the figure.

estimates can only be made based on more detailed geological modelling in combination with numerical flow simulations. The geophysical modelling of Johansen and surrounding formations suggests good sandstone properties for Johansen. Permeabilities within the (whole) formation range from 64 to 1660 mD, see Figure 5 for an extracted sector model of Johansen. Together with the vertical and lateral extent of the formation this indicates good injectivity, but this will also be an issues when planning the injection well location.

3. DESCRIPTION OF DATASET AND SIMULATION SET-UP

One of the main purposes of this paper is to present a complete dataset for the Johansen formation, for which simulation of CO_2 injection may be performed. Our fluid flow simulations are limited to two-phase immiscible flow. However, the dataset is made accessible in such a format that other research groups may perform more detailed simulations, for instance solubility of CO_2 in brine/water. The format of the data is not unique to a particular simulator.

The geometry of the formation is made available at the web-site [11], together with porosities and permeabilities, and fluid data to be described below. A summary of the files which are made available, is given in Section 3.3. The simulation grid is given in Corner Point format, see for instance [12] and [25]; and a brief description of this format given below. Two-phase flow is utilized by a dataset for relative permeability of the water phase and the CO_2 phase. PVT data is supplied based on properties of water and CO_2 at constant temperature 94 degrees Celsius.
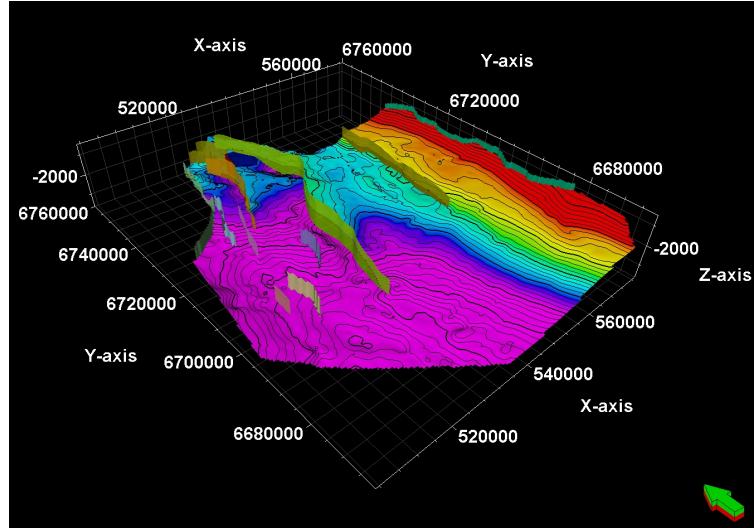
FIGURE 4. Representation of one of the horizon surfaces of a geological layer. Main vertical faults are shown as green bands. Lateral coordinate axes represent longitudinal and latitudinal coordinates. Vertical axis represents depth below sea level, and the levels are indicated by the contours on the horizon surface.

A single injection well is used in the simulations to account for the injected CO_2 corresponding to the location where injection is most likely to be performed. This penetrates the whole Johansen formation (vertically) at the chosen location. The positioning of an injection well is discussed in more detail below. The injection rates will be set to 3.5M tonnes CO_2 per year. This is somewhat more than the combined CO_2 emissions from Kårstø and Mongstad.

The geological model for the Johansen formation and the sedimentary sequences above and below are based on geologist's interpretations of horizons of geological layers, see Section 2. An example of an interpretation of one horizon is shown in Figure 4 together with the main vertical faults of the model. Within the layers, geological modelling has been performed. Petrophysical data, such as porosity and permeability, has been modelled from seismics and by well correlations. At the time of making the data available, no geological facies model was available. A geological grid is constructed from the definition of horizons of geological layers. Specifically, the main sequence of geological zones from top to bottom is given by:

(1) Top Sognefjord
(2) Sognefjord shale
(3) Fensfjord formation
(4) Krossfjord formation
(5) Krossfjord-Brent group
(6) Brent group
(7) Dunlin group
(8) Johansen formation (thickness varies between 80 m and 120 m).
(9) Amundsen shale
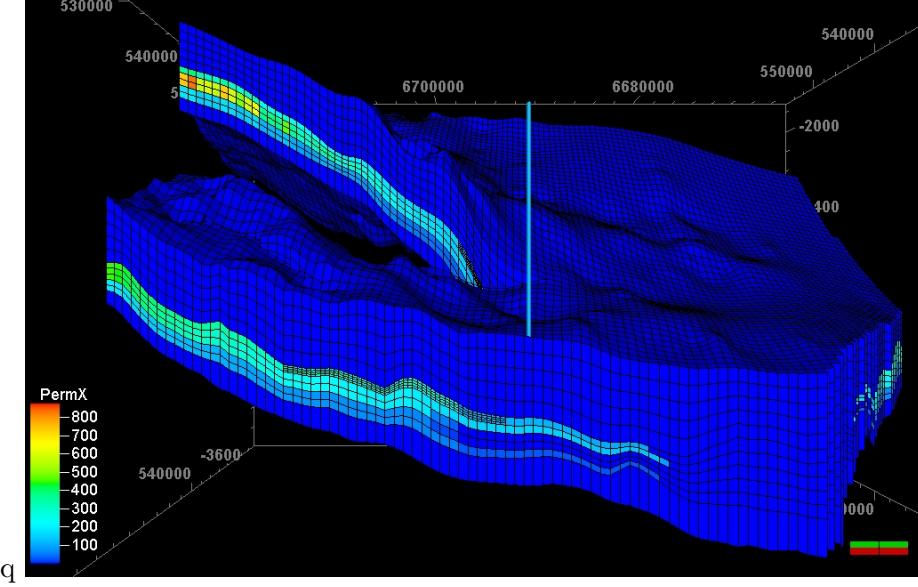
FIGURE 5. Permeability representation shown within sector of Johansen formation. Shale above and below Johansen are represented by 5 and 1 grid layers respectively.

(10) Statfjord formation

Some of these are divided into sub-zones so that the total model consists of 16 geological zones. In particular, the Johansen formation contains three sub-zones. The lateral extent of the entire model is approximately 75 km × 100 km.

To limit the number of active grid cells in our study, CO_2 injection is simulated only in the sector model shown in Figure 5. This sector consists of the lower 3 geological zones (Amundsen, Johansen, Dunlin). Figure 5 shows the permeability description within the sector model, where the Johansen formation has been represented by 5 layers of grid cells. The lowermost layer corresponds to the Amundsen shale, and the 5 layers above Johansen correspond to the grid representation of the Dunlin shale. Notice the main fault that divides the Johansen into two parts. The location of the injection well is in the area south-west of the the main fault and where CO_2 may move into the areas to the east of the fault. Since the geological model indicates that the faults are sealing when the fault throw is large we do not consider vertical flow in the faults towards shallower regions. Flow of CO_2 through the vertical faults has been investigated in [6] by incorporating fault transmissibility multipliers in their model, and studying injection points further north, closer to Troll. The original dataset and corresponding grid, are made available on the web-site [11], and may be used to investigate faults as pathways for leakage in further studies.

The actual position of an injection well for full scale CO_2 handling has not been decided yet. Currently seismic modeling is performed to get better data for geophysical properties of Johansen, and these will be important for the choice of injector position. Issues to be considered when choosing an injection point

are related to injectivity, to CO_2 not flowing into higher parts of the formation, and also to avoid CO_2 moving into areas near faults with uncertain sealing properties. The location of the Troll field will also affect the choice of injection point.

Within both the Dunlin shale and the Amundsen shale, constant values are used for permeability; respectively 0.01 mD and 0.1 mD ($1D = 9.86910^{-13}m^2$). The permeability of the Johansen formation varies between 64 and 1660 mD. The permeability data are based on well interpretation, and depth correlations as described in Section 2. Figure 5 shows the vertical grid representation (with permeability values) at a cross section within an extracted sector model, seen from west toward east.

The grid is represented in corner point format [25]. This format is an extension of the logical Cartesian grid format. Due to the vertical faulting of geological zones seen from Figure 5, the corners of grid cells are in general not conforming from one grid block to the neighboring grid block. The corner point format assumes that grid cell corners are distributed along vertical pillars. All grid cells have 8 corners, but these may not be distinct due to grid pinch-outs. Since the grids are allowed to contain vertical faults, all the eight corners are provided for each grid block. This results in voluminous data. Section 3.3 contains a listing of the files where the geometry of the grids are provided. Grids are provided for both the entire model and the sector model seen in Figure 5. The coarsest grid used in the simulations is a $100 \times 100 \times 11$ corner point grid. The typical cell size for this grid is 500m $\times$ 500m laterally, and 16 to 24 m vertically.

3.1. **Discretization techniques.** The simulations presented here are based on the industry standard black oil simulator Eclipse 100 [12]. This simulator is based on a control-volume formulation of the governing equations. In this formulation each grid block i will be a control volume V_i such that mass balance is satisfied for each fluid phase α:

$$(1) \qquad \int_{V_i} (\frac{\partial(\phi\rho_\alpha)}{\partial t} + \nabla \cdot (\rho_\alpha \boldsymbol{v}_\alpha))dV = \int_{V_i} q_\alpha dV,$$

where the following quantities are introduced: ϕ porosity; ρ_α phase density; q_α source or sink terms for fluid phase α. The Darcy velocity $\boldsymbol{v}_\alpha$ for phase α is given by

$$(2) \qquad \boldsymbol{v}_\alpha = -\frac{\boldsymbol{K}k_{r_\alpha}}{\mu_\alpha}(\nabla p + \rho g \nabla z).$$

Here $\boldsymbol{K}$ is the permeability/conductivity of the porous medium, k_{r_α} is the relative permeability for phase α, μ_α is the viscosity of phase α, p is the pressure, g is the gravitational constant, and z denotes the height above some depth reference point. Capillary pressure is neglected for simplicity.

We will consider three types of boundary conditions. These are introduced in Section 4.2 together with their practical implemetation.

3.1.1. *Transmisibility calculations.* Fluxes are discretized for all cell faces of a grid block. A common discretization technique, e.g. used in [12], is the two-point flux approximation (TPFA) method. In this method single phase fluxes across grid block faces are be approximated by

$$(3) \qquad\qquad f_i = t_i(u_{i-} - u_{i+}),$$

where u_{i-} and u_{i+} refer to the fluid potentials at the grid block nodes on either side of the grid block face. The coefficient t_i denotes the transmissibility associated with the grid block face, and is essentially calculated from local geometry and permeability, cfr. [1]. Multi phase flow is handled by upstream weighting of relative permeability. When the grid blocks are faulted with respect to each other, the transmissibility coefficients are modified, see [2], [3], [17], and larger cell stencils for the discretized mass balance equations may occur. If there is communication between layers that have been faulted with respect to each others through faults, so-called non-neighbour connections may be set up. This means that the indexing of the fluid potentials in Eq. (3) may be generalized to account for grid cells that are not 'logical' neighbors, so that flows across grid block faces are governed by non-neighbouring cells.

Multi point flux approximation methods (MPFA), are more general transmissibility calculation techniques when more grid block/control volumes are used to approximate fluxes, see [1], [2], and [3].

The concept of *transmissibility multipliers* allows for modifications of the discrete fluxes in Eq. (3), see for example [17], and is often used for history matching in practical reservoir simulation. The transmissibility t_i is multiplied by a factor to either increase or decrease the flux across the cell phase. Layers that are 'neighbours' across a fault, may be assigned a small transmissibility if flow is reduced across the fault. The faults in our simulation grids are predominantly sealing due to the high clay content in Dunlin shale, so that transmissibility reduction factors are used in Eq. (3). The dataset contains files with transmissibility multipliers produced from the fault handling in [12].

Various methods exist for calculations of transmissibility multipliers based on local geometry in the vicinity of the faults and the local geological properties. More detailed knowledge of the geology, such as clay content, fault smearing, fault throw and orientation of fault zones may also be included in calculations of multipliers [17]. In Figure 6 we have shown calculated fault transmissibility multipliers for the main faults, based on clay content and fault displacement from the entire geological model.

An example of fault transmissibility multipliers for the sector model is provided in Figure 7, which shows multipliers for the part of the main fault between the layers included here.

Fault activation due to pressure build-up constitutes potential risks for leakage out of the formation, [4]. In the case of the Johansen formation, CO_2 may then flow to layers of sandstone above the formation, and further up to the Troll field or surrounding media. Leakage of CO_2 to the formations above the Johansen formation has been investigated in [6] by studying various fault transmissibility options for a full model.
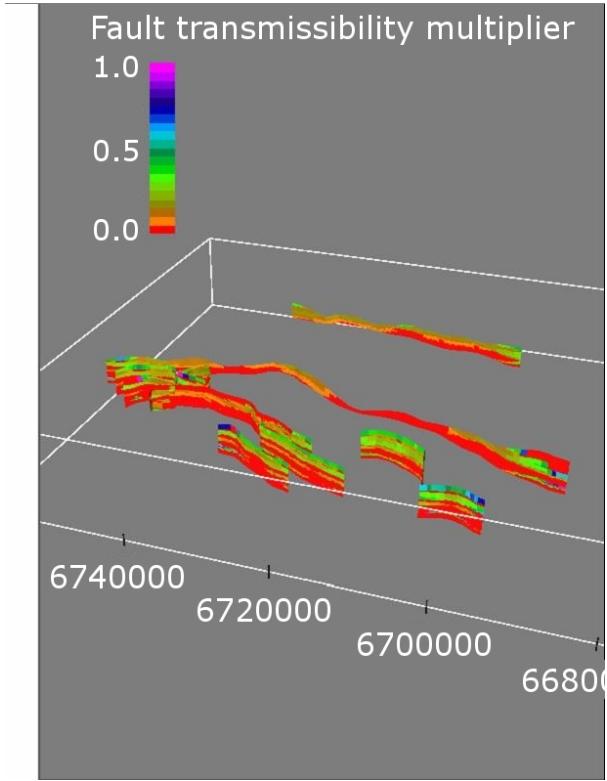
FIGURE 6. Fault transmissibility multipliers calculated for the major faults in the full geological model, as seen in Figure 4, based on clay content of Dunlin shale in combination with Johansen sandstone properties and fault throw.
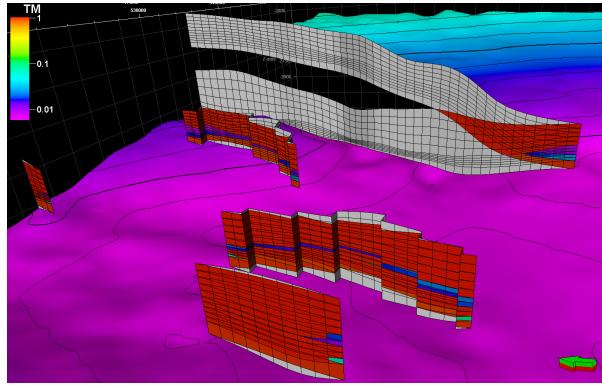
FIGURE 7. Transmissibility multipliers of the faults used in the sector model. Horizon of one of layers shown together with discrete representation of vertical faults.

3.2. **Fluid data.** The dataset presented here provides geometry, geology and petrophysical properties for a realistic storage site. We consider two-phase immiscible flow with CO_2 being the nonwetting phase, and the resident brine
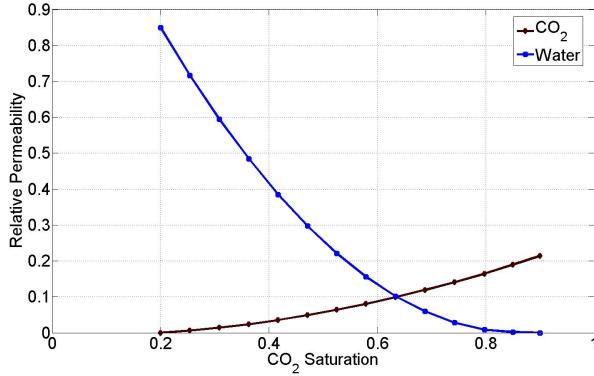
FIGURE 8. Relative permeability curves for CO_2 and water, with residual brine saturation, $S_{rb} = 0.1$, and residual CO_2 saturation, $S_{rc} = 0.2$.

being wetting. The phases are isothermal, compressible, and have densities and viscosities that vary with pressure. Isothermal PVT data at 94 degrees Celsius are generated from the web-based database NIST [16] for pressure values in the pressure regime that exists during the simulation time. As an example, at 250 bar pressure supercritical CO_2 has a density of approximately 617 kg/m^3, and viscosity 0.049 cP. This should be compared to water density of 973 kg/m^3 and water viscosity of 0.307 cP for 250 bar. Tables with varying PVT data are further presented in the online data-set [11], and a description of the files is provided in Section 3.3. Relative permeability data consists of a set of water and CO_2 curves, where the residual water saturation is $S_{rb} = 0.1$ and residual CO_2 saturation is $S_{rc} = 0.2$. The relative permeability curves for water and CO_2 used in this dataset are plotted in Figure 8. In this study we do not account for hysteresis in residual CO_2 saturation values which generally depends on the sweeping history, see for instance [13]. However, the effect of varying the end-points of the relative permeability curves is investigated in Section 4.4.

Capillary pressure has been neglected in this study, but it should be emphasized that core data treatment to determine both relative permeability and capillary pressure is an important issue, and of particular interest for long term behavior, and fluid propagation after the injection phase.

3.3. **Data file descriptions.** Datafiles are made available on the web-page [11]. A brief description of datafiles is provided below. The web page will contain a more detailed description of data included and specific files. Additional information is also included in file headers.

Geometry files:
Grids are made available in corner point format, see [25]. The entire model is discretized by a $155 \times 160 \times 16$ grid. This grid describes all zones and the entire lateral domain. The Johansen formation is given by 3 layers.
The sector models correspond to the south western parts of the geological domain. The sector models are discretized by a 100×100 lateral grid and by

(1) 5 layers, (2) 10 layers, (3) 15 layers representation of Johansen formation. The shale (Dunlin) above Johansen is represented by 5 grid layers in all sector models.

Petrophysical data files:
Petrophysical data is given for the entire model, and for the sector models with different vertical grid representation corresponding to geometry files above.

Fault data files:
Logical fault definitions are given corresponding to files above. Non-neighbour connections and fault transmissibility multipliers are provided for the different grids.

Fluid data files:
Fluid data is given for an immiscible water-CO_2 system at isothermal conditions. PVT data is given for 94 degrees Celsius.

Well data files:
Well positioning is given in global coordinates. The rates are constant during the injection period, and the well has vertical perforation through the Johansen formation.

4. Simulation of CO_2 injection in the Johansen aquifer

The aim of this Section is to study some modeling factors that we believe are important for the CO_2 saturation distribution in the formation, and consequently for the storage capacity estimation. For a complete study of storage of CO_2 and risk modeling, a much more detailed study must be performed.

The sector model includes shale both above and below the Johansen formation itself. In particular, the Johansen formation is limited upwards by the Dunlin shale/group, see Section 2 for more details.

All examples are simulated with the Eclipse 100 simulator [12]. Simulations are performed for various grid representations of the sector domain. Boundary conditions and permeabilities will be specified for the various examples. Fluid data is described in Section 3, and is the same for all examples. Faults and transmissibility calculations are handled internally in the simulator for the various geometry and permeability files. The initial water pressure for the simulations is assumed to be determined by hydrostatic equilibrium, indicating pressures around 250-310 bar within the simulated sector model. Fluid flow is simulated on a lateral sector of the geological model in the south-westernmost part of the Johansen formation. This sector is described in detail in Section 3.

Initially we give an example of simulation of CO_2 injection in the Johansen formation, together with a simplified CO_2 inventory study. Then the effects of lateral boundary conditions, grid resolution, and relative permeability description are studied. Finally some simulations with varying permeability models are presented.
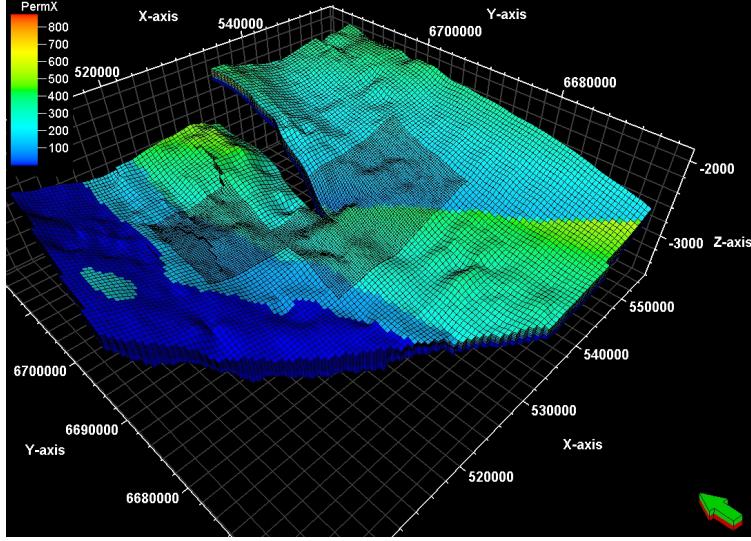
FIGURE 9. Simulated sector model. Local grid refinement is applied to region of particular interest. Permeability model from approach described in Section 2.

4.1. **Example of simulation set-up and CO_2 time development.** This example is used to illustrate CO_2 injection in a sector model of the Johansen formation and time development of the injected CO_2. The geometry is taken for the 5 layer sector model, described in Section 3. Porosities and permeabilities are calculated based on the geological modelling described in Section 2, and the permeabilities in the uppermost grid layer of Johansen are depicted in Figure 5. The sector model is a $100 \times 100 \times 5$ grid cell description of the Johansen layers, and further 5 grid layers of shale above the Johansen formation, and 1 grid layer of shale below. As described in Section 2, the shale layers above Johansen stem from the Dunlin group, and the shale below is the Amundsen shale. Boundary conditions are given as no-flow, but where the volumes of the grid blocks of the boundaries have been multiplied by a factor 1000, as described in Section 3 and Section 4.2 below. Fault transmissibilities across grid block interfaces neighboring the main vertical fault are calculated by internal transmissibility calculations of the simulator [12], see also Figure 7. Flow from west to east in the simulation grid will mainly occur in the southern parts of the fault where the Johansen layers are physically connected. Due to the coarse main grid description we use local grid refinement in an area of the domain that is swept by CO_2. The grid resolution factors are 2×2 laterally, and 4 vertically. Given a typical coarse grid cell size of $500m \times 500m \times 20m$, the typical grid size of refined cells is $250m \times 250m \times 5m$. The local grid refinement is applied to parts of the uppermost grid-layer of Johansen. The sector grid and permeability representation are illustrated in Figure 9. The position of the injection well is chosen to be far south and west of the main vertical fault illustrated in Figure. 5. Injection rates of approximately 3.5 Mt CO_2 per year are used. Relative permeability data is taken from Figure 8, and the PVT data for a

water-CO_2 system is discussed in Section 3. CO_2 is injected for 110 years, and the time development is simulated for a further 400 years after injection-stop to demonstrate the effects of buoyancy driven flow.

The time development of the CO_2 in the uppermost layer of Johansen is plotted in Figure 10, where the saturation profiles are plotted at 110, 210 and 510 years together with the injector position. As time develops, the CO_2 flows to the upper parts of Johansen, and leaves a trail of immobile CO_2 behind. In addition, some CO_2 is trapped in local stratigraphic traps or domes.

Figure 11 is used to illustrate the storage mechanisms in an area around the injector. We have extracted a $12 \times 12 \times 5$ box region surrounding the injection well. The CO_2 volumes in place are plotted for this region as a function of time. The volumes increase as the injection is started. When injection is stopped after 110 year, the volume in place starts to decrease because CO_2 continues to move out of the region due to buyoancy. However, not all CO_2 will leave the region due to residual, and local stratigraphic trapping of CO_2 The residual trapping is accounted for by using residual CO_2 saturation $S_{rc} = 0.2$ in the imbibition relative permeability curve.

4.2. **Impact of boundary conditions.** Boundaries of the sector model may be handled by either accounting for fluxes or pressures at the lateral boundaries, or by modifying volumes of boundary cells to account for volumes that have been left out from the entire model. The boundaries above and below the shales are treated as no-flow boundaries since the shales are thick above the Johansen formation in the extracted sector region. We omit issues related to flow parallel to vertical faults. Varying boundary conditions above the shales would have a significant impact if there are permeable paths within the shales or within the vertical faults that exist in the model.

Second to the sealing properties of the cap rock, the lateral boundary conditions must be dealt with properly in the simulation model, although little is currently known for the Johansen formation. There are various ways of specifying boundary conditions for the fluid flow simulations, based on knowledge of pressure support or known in/out-fluxes to/from a formation. We first study the effect of various boundary scenarios that may be used for the chosen simulator [12], and investigate the pressure build-up. These boundary conditions are quite general and may be included in other fluid flow simulators. Three main cases are studied:

> **BC1:** No-flow boundaries with pore volumes of boundary cells greatly increased using pore volume multipliers. This condition mimics the effect of the boundary being far away from the injection point and largely governed by the initial pressure of the boundary cells. In the simulations the pore volume multipliers are set to 1000, which corresponds to the number used in [13]. The modification of pore volumes implies that the volumes for the cells along the boundary are adjusted in Equation (1) for the governing cells, while maintaining no-flow across boundary faces. The no-flow condition for boundary faces is formally given by $\int_{\Omega_j} \boldsymbol{K} \nabla u \cdot \boldsymbol{n} = 0$ for all cell faces j on the boundary, where $\boldsymbol{K}$ is the
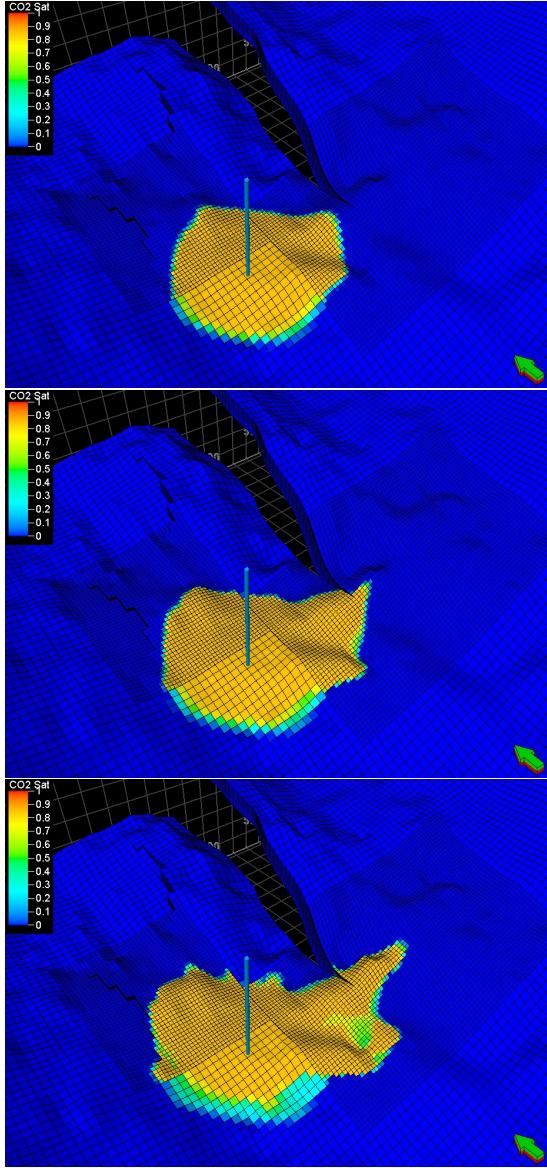
FIGURE 10. CO_2 saturation development for simulation set-up in Section 4.1 in upper grid layer of Johansen. Uppermost plot; saturation profile after 110 years (injection stop). Middle plot; 210 years. Lowermost plot; 510 years. Notice that CO_2 reaches the main vertical fault during the simulation period, which may constitute leakage scenarios higher up in the formations through the fault.

permeability of the grid cell, $\boldsymbol{n}$ is the outward normal vector of the bounday face, and u is the fluid potential.

BC2: Grid cells at parts of the lateral boundary are assigned pressure driven production wells, while the boundary edges of boundary cells employ a no-flow condition. The constraints on the artificial wells are
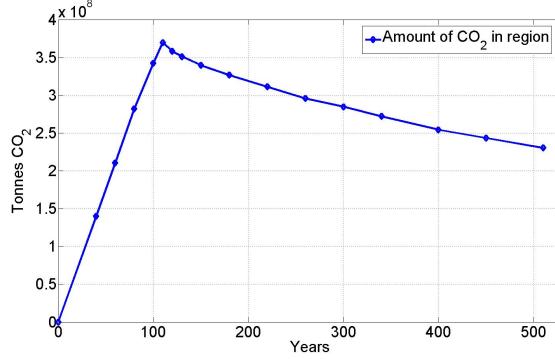
FIGURE 11. Amount of CO_2 within box region surrounding injection well vs. time. Amount increases linearly with the injection rate until CO_2 reaches boundary of the box region. Afterwards a decrease is observed. Asymptotic trend indicates effect of trapping of CO_2 within the box, and is a combination of residual trapping and stratigraphic traps.

set such that almost the same injected volumes are being produced initially. This relies on modification of the well term q of Equation (1) for cells containing wells. Specifically, here we employ two production wells (pressure driven, constant pressure of 270 bar) near the main fault, in the western part of the Johansen area. The reason for choosing these positions is to show the possible communication with layers higher in the formation through the main vertical fault by triggering movement of CO_2 towards the areas near the main fault.

BC3: Boundary conditions specified through reservoir contact with external aquifers. This boundary treatment option is commonly used in practical reservoir simulation. The aquifer contact can be represented either numerically or analytically. In the analytical case, the aquifer is represented through source terms in a specified set of boundary grid cells. Various models exist for computing the source terms. In our case, we have used the Fetkovich aquifer model which assumes a pseudosteadystate flow regime between the aquifer and the reservoir. The aquifer inflow rate is specified by a Darcy law type expression, while the pressure response in the aquifer is given by a material balance expression. We refer to [12] for more details on external aquifer representation.

In Figure 12 the bottom hole pressure (BHP) for the injection well has been plotted versus time for the simulations with the boundary conditions above. The medium is described by homogeneous permeability (500 mD), and a 10 layer grid representation is employed throughout the Johansen formation. Relative permeability curves are shown in Figure 8, and the fluid data is the same as in Section 4.1. As can be seen from the plot, the BHP initially experiences a sharp transient response lasting for about 5 years. This transient consists of a rapid pressure increase of approximately 10-12 bar followed by a pressure decrease. A slow long term increase of the BHP in Figure 12 is due to
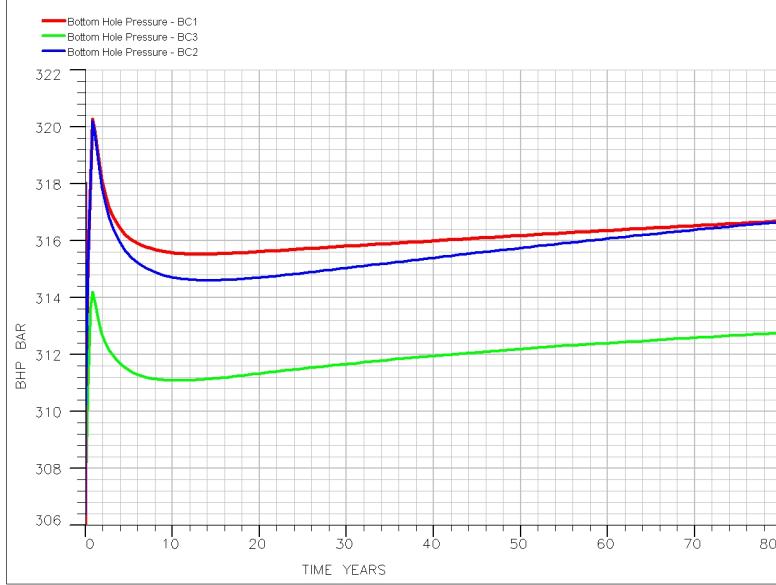
FIGURE 12. Bottom hole pressure (BHP) versus time for different boundary conditions: Red curve corresponds to no-flow boundaries with increased pore volumes at boundary cells (BC1); Blue curve to flux/pressure control in boundary cells (BC2); Green curve to aquifer support (BC3).

net accumulation of fluid inside the formation. Although these conditions give comparable results we note that the aquifer support condition, BC3, gives the lowest BHP increase. This, however, depends on how the aquifer options are applied [12]. The formation pressure build-up may be a very important since it can lead to fracturing and fault activation, see for example [6].

The CO_2 saturation distributions after 510 years simulation for each of these boundary conditions are shown in Figure 13. As can be seen from the figure, there is little difference between the case with pore volume multipliers and the external aquifer support, BC1 and BC3 respectively. In these cases the CO_2 saturation distributions are determined mainly by buoyancy effects, local topology of the layers, and the inherent effect from juxtaposition of layers and the impermeable cell faces of these due to shale in the faults. As expected the CO_2 saturation for the flux/pressure condition (BC2) is quite different from the results obtained using the other types of boundary conditions. This result does not only depend strongly on the conditions chosen for each of the artificial wells, but also on their location. In this case, since the location of the artificial producers is at the western part of the main fault, more CO_2 moves into the western part of the formation.

4.3. **Grid resolution and distribution of CO_2 plume.** Due to computational demands on the fluid flow simulator, the issue of grid coarsening arises naturally and will limit the number of grid cells used in a simulation model. Whereas the geological grid may contain much more detailed information about
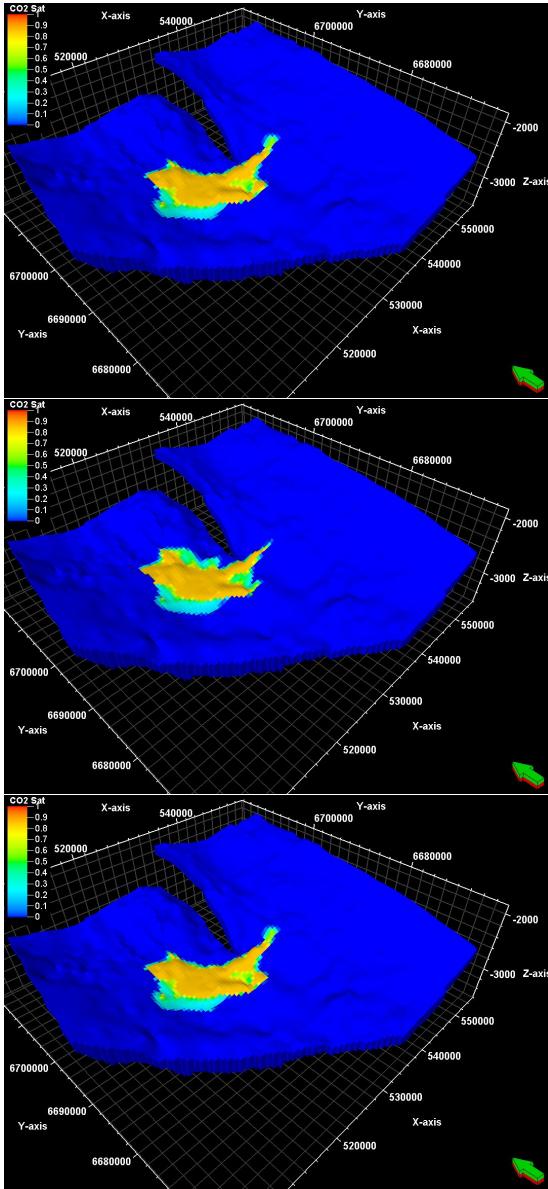
FIGURE 13. CO_2 saturation distributions after 510 years (110 years of injection; thereafter 400 years post injection period). Uppermost figure corresponds to no-flow boundaries with increased pore volumes at boundary cells (BC1). Middle figure corresponds to flux/pressure control in boundary cells (BC2). Lowermost figure corresponds to aquifer support (BC3). Homogeneous permeability description (500 mD), 10 layer grid representation of Johansen. Grid lines are not included for visualization purposes.

geometry and geology of the formation, geometry and permeabilities must eventually be up-scaled to a representative simulation grid. An important issue to consider from a modelling and simulation perspective is the effect that coarsening has on the CO_2 saturation distribution when accounting for relative permeability, capillary pressure and PVT data. The shape of CO_2 plumes has been studied, e.g. in [18], [19], [20], and suggests that a certain level of grid resolution must be employed to incorporate the effects of nonlinearities. In particular, we must expect to provide sufficient grid resolution in the vertical direction.

To simplify the study of grid resolution effects on the CO_2 saturation distribution, we use homogeneous permeability within the Johansen formation and the neighbouring layers. The permeability is set to 500 mD in Johansen, and low permeability values are used for the Dunlin shales/group as described in Section 3.

The shales above and below the Johansen formation are represented respectively by 5 and 1 layer(s) of grid cells. Within the Johansen formation we consider three different vertical grid resolutions in the 5 layer model, and we investigate different local grid resolutions in the areas which will be flooded by CO_2. The areas with local grid refinement (LGR) are the same as in Figure 9. The first grid has no refinement, the second has 2×2 local refinement laterally, and 4 cells vertically. The third grid has local refinement 3×3 laterally, and 8 cells vertically.

In Figure 14 the simulation cases are presented. The CO_2 saturation distribution in the top layer is plotted after 110 years of injection followed by a 400 year post-injection period. As can be seen from the plots, the distribution of CO_2 differs significantly. The lateral spreading of CO_2 in the uppermost layer of the Johansen formation covers a much larger area when using the finer grids. The major difference is between coarse grid and the refined grids. The difference between the $2 \times 2 \times 4$ LGR and $3 \times 3 \times 8$ LGR is much smaller, and indicates that the $2 \times 2 \times 4$ LGR representation in the upper layer is reasonably accurate for simulation of CO_2 injection in this particular case. Note, however, that we have not performed a detailed convergence study of the grid resolutions. Although this example mainly accounts for flow within the Johansen formation, grid resolution issues are important to be aware of when simulating CO_2 movement in a full model. Needless to say, if a high level of grid refinement is needed in the simulation grids, the computational demand may be severe.

It is observed in the simulations that some CO_2 migrates up into the first layer immediately above Johansen. After 510 years the maximum saturation in this grid layer of shale is approximately 5 percent. In the grid layers above we observe no CO_2. The reason why CO_2 moves into the shale in the numerical simulations is dependent on the relative permeability representation. Specifically, since upstream weighting of relative permeability is used by the simulator, some of the CO_2 movement into the shale is a purely numerical effect. This discretization technique then leads to an over-estimate of CO_2 volumes in the lower parts of the shale. Due to the very low permeability values at saturation values near critical CO_2 saturations, the movement of CO_2 to the shale grid layers higher in the formation will be almost zero. In our relative permeability model, as indicated by Figure 8, the relative permeability values at 5 percent
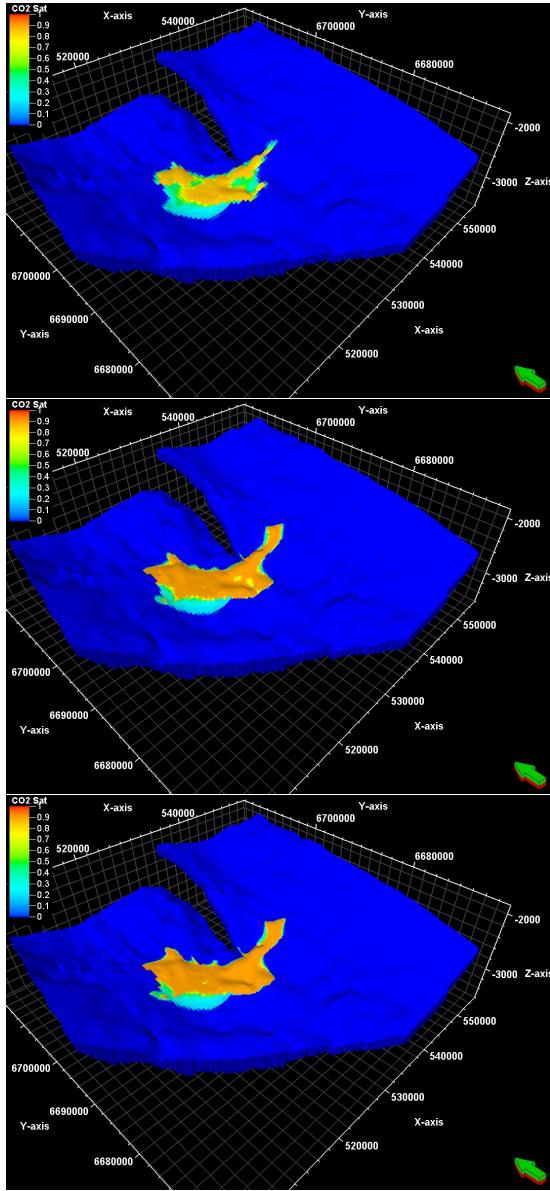
FIGURE 14. Simulation of CO_2 migration with various grid resolution in the uppermost layer of the Johansen formation. CO_2 profile after a total simulation period of 510 years. Uppermost plot; 5 grid layer representation of Johansen with no refinement. Middle; 5 layers combined with local grid refinement factor of 2 laterally and 4 vertically in upper grid layer. Lowermost plot; 5 layers combined with local grid refinement factor of 3 laterally and 8 vertically in upper grid layer. Grid lines not plotted for visualization purposes.

are actually zero, and no movement further up in shale is seen. Since we have represented the shale by 5 grid layers here, this impairs overestimated volumes of CO_2 higher in the shale zones. Grid representation of shale will also affect the CO_2 movement/migration in a full field model where transport of CO_2 is allowed due to fault transmissibility modifications, and care must be taken not to make conclusions about CO_2 migration and leakage that are biased by the numerical simulation techniques.

4.4. **Impact of relative permeability.** To illustrate the effect of residual saturation, the saturation distributions at the time when injection is stopped (110 years) is compared with the distribution 100 years later. The simulation grid is the 10 grid layer representation of Johansen with homogeneous permeability. Relative permeability curves from Figure 8, and BC1 have been employed.

Two notable effects are seen from the plots in Figure 15. After end of injection, CO_2 will continue to move upwards due to buoyancy, and displace water. In the plotted regions, CO_2 has flooded areas close to the injection point. When CO_2 continues to move upwards from flooded areas, CO_2 will eventually be trapped due to the residual CO_2 saturation value used in the definition of relative permeability curves. This leaves a trail of residual and immobile CO_2 phase, as seen in Figure 15. In our example calculations the residual CO_2 saturations are set to 20 percent. However, experimental values close to 40 percent have been reported in the literature [4]. Storage capacity estimation is of course very sensitive to the value of residual CO_2 saturation. Rock property models may be a major uncertainty for North Sea geological formations. The effect of varying relative permeability data is illustrated by the following example. Consider the relative permeability curves (1), (2) and (3), shown in Figure 16, with curve explanation in the figure text. The fluid data is the same as the previous examples, homogeneous permeability of 500 mD and 10 grid layers are used for Johansen. Saturation profiles are plotted in Figure 17 for each case. As seen from the figures, the fronts spread quite differently depending on the permeability description. The most spreading of CO_2 is seen when using the relative permeability Curve (2). This relative permeability curve is obtained by scaling Curve (1) corresponding to the original relative permability curve for CO_2 given in Figure 8 by a factor 2. Larger areas will also be swept by the primary drainage Curve (3) compared to the original realtive permeability Curve (1), since no residual CO_2 is left in place in this case. In this case we also observe that more CO_2 moves into the parts west of the main fault. The relative permeability description will be important for leakage scenarios since the end-points and form of these curves alters the front speed and sweep areas of the CO_2 plume. This may lead to faster arrival to potential pathways upwards in the formation, and possibly also faster migration in faults.

The effects of relative permeability hysteresis for CO_2 modelling are studied in [13]. Mainly hysteresis will alter the shape and speed of the propagating front. From Figure 16 we see that the relative permeability of CO_2 is larger when $S_{rc} = 0$ (Curve (3)) than when $S_{rc} \neq 0$ (Curve (1)). Consequently, the front of the CO_2-plume will flow faster when the residual CO_2 is zero. This is
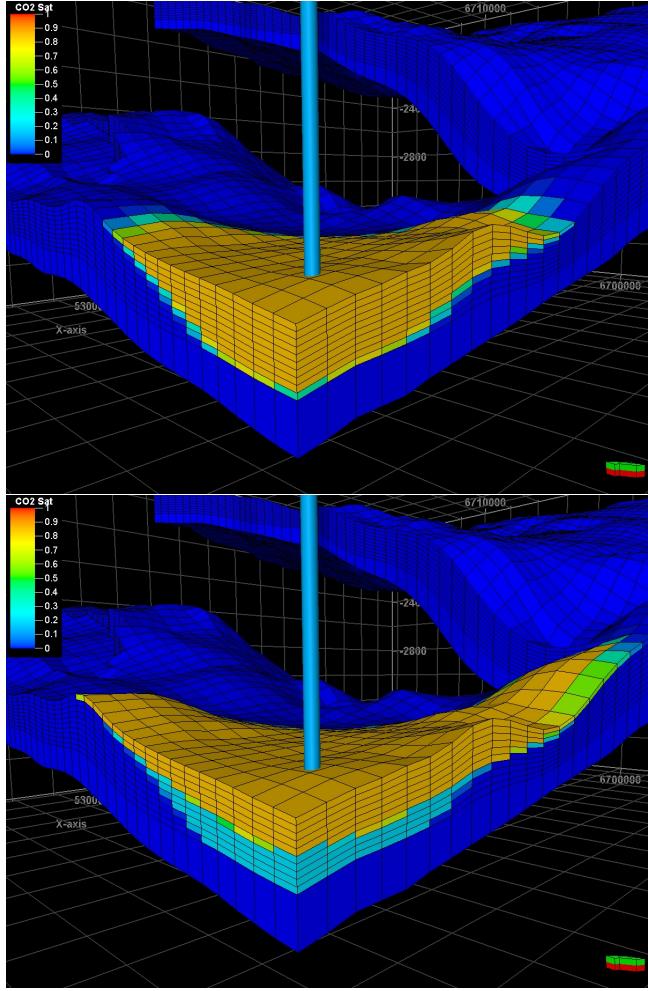
FIGURE 15. CO_2 saturation distribution in a region near the injection point. Upper Figure: CO_2 saturations after 110 years of injection. Lower Figure: CO_2 saturations 100 years after injection was stopped. Residual CO_2 saturation of 20 percent, and curves from Figure 8 applied. Approximate thickness of grids cells is 8-10 meters.

also observed in the simulations. The effect of trapping in a hysteresis model as compared to a model with fixed residual saturation, $S_{rc} \neq 0$, see Figure 8, would primarily be that less CO_2 may be trapped when the hysteresis curves are used. For areas that have been flooded by CO_2, but where maximum CO_2 saturation has not been reached, the residual CO_2 saturation will be less than S_{rc} if drainage is reversed to imbibition for these grid blocks.

4.5. **Impact of permeability description.** The chosen injection point in this study is in the south-westernmost location of the Johansen formation. The heterogeneous permeability model described in Section 2 was employed in the simulation example in 4.1. Possible injection positions further north toward
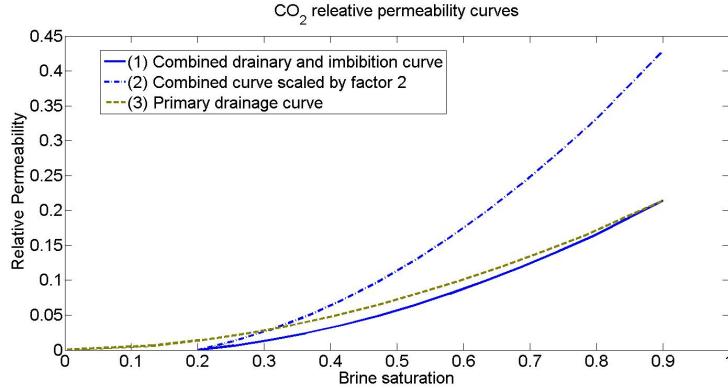
FIGURE 16. Different relative permeability curves for CO_2: Curve (1) is identical to the curve given in Figure 8 with residual brine saturation $S_{rb} = 0.1$, and residual CO_2 saturation, $S_{rc} = 0.2$; Curve (2) is obtained by shifting the end-point relative permeability at residual brine saturation by a factor of 2 (this scales Curve (1) by a factor 2); Curve (3) represents primary drainage and is obtained by shifting residual CO_2 saturation to $S_{rc} = 0$;

the Troll area would be in regions with higher permeability values in the geological/geophysical model. This motivates testing different permeability descriptions with larger values in this example. We employ the 5 layer simulation grid for the Johansen formation, described in Section 3. Local refinement is used in the same areas as in Example 4.1, and relative permeability curve (1) is taken from Figure 16. The first permeability model is the heterogeneous model from Example 4.1, the second uses homogeneous permeability of $500mD$ in the entire area of Johansen, and the third used homogeneous permeability of $1000mD$. The simulated CO_2 profiles are plotted in Figure 18. As can be seen, the front moves much further with the largest values for the permeability, and much larger areas are swept by CO_2. As a consequence, the effects of residual CO_2 trapping are much more profound for larger values of permeability, and several local domes are observed with CO_2 trapped in stratigraphic traps. From a storage point of view, the trapping effects have a positive effect. However, due to sweeping larger areas, there is an increased risk of CO_2 moving into more faulted regions where leakage into formations above the Johansen formation could occur.

5. CONCLUSIONS

The Johansen formation is a deep saline aquifer located offshore the west coast of Norway. The aquifer is a candidate site for large-scale handling of CO_2 emissions from future gas power plants. This paper describes a dataset for the geological model. The dataset can be dowloaded together with fluid properties. The geological model has been described in detail, and some simulation results have been shown for injection of CO_2. These simulations have been performed using the industry standard simulator Eclipse 100, and can be used as a basis
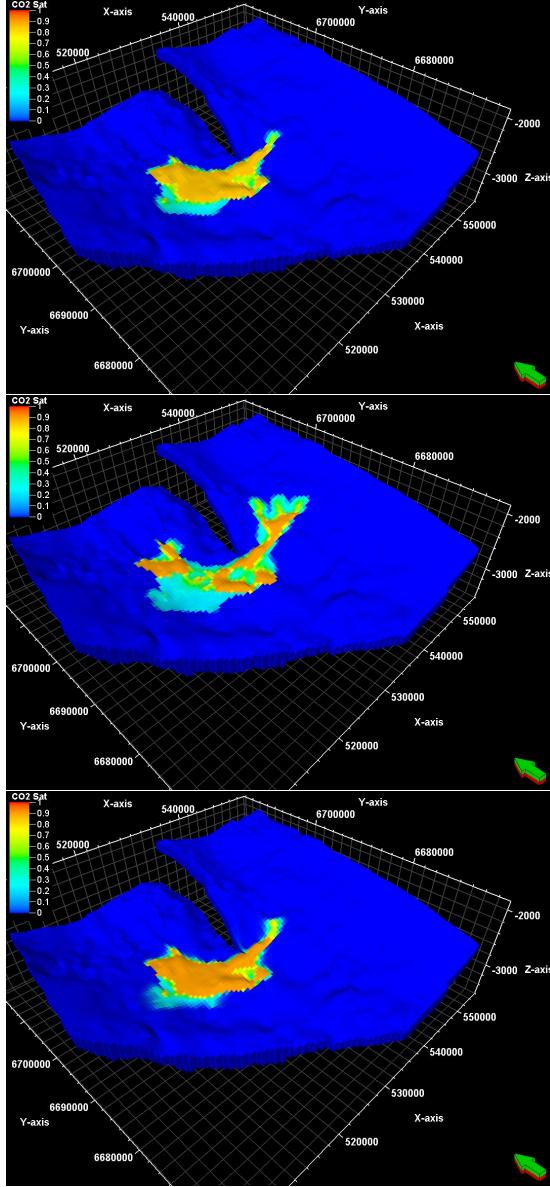
FIGURE 17. CO_2 saturation profiles simulated with the three different relative permeability curves shown in Figure 16. Simulated profiles plotted in uppermost grid layer of Johansen after 110 years of injection followed by 400 years of post injection. The top figure corresponds to Curve (1) in Figure 16; The middel figure to Curve (2); The bottom figure to Curve (3);

for comparisons. The geological model has been used to perform various simulations of CO_2 flow and transport based on realistic injection scenarios. We show that the choice of lateral boundary conditions may significantly change the simulation results. Furthermore, we show that vertical grid refinement is
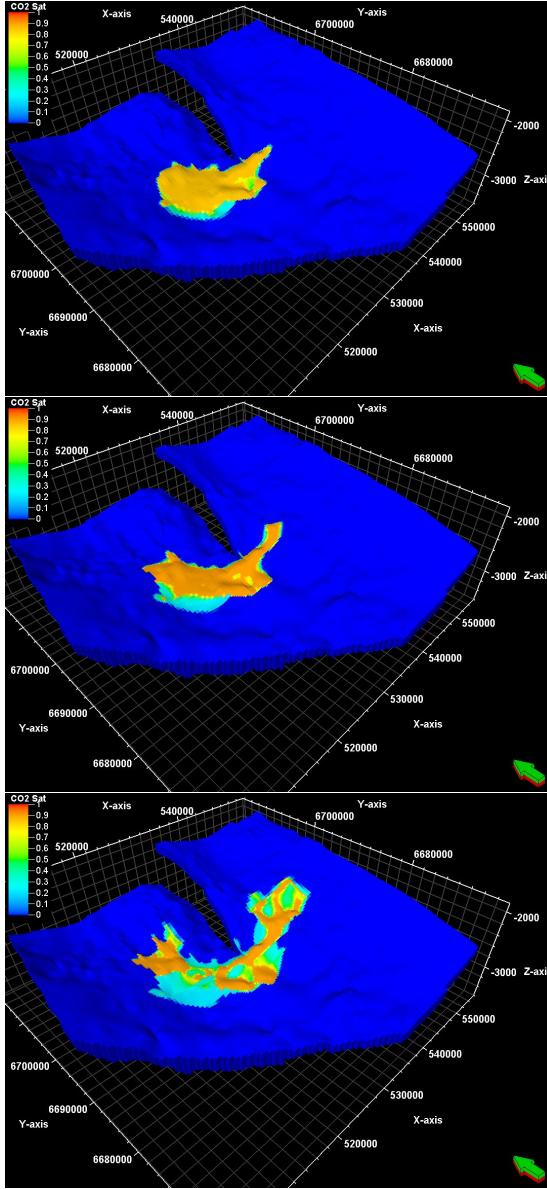
FIGURE 18. CO_2 saturation distributions after 510 years of simulation for three different permeability representations of the Johansen formation. Saturation profiles plotted in the top grid layer of Johansen. Top; heterogeneous permeability model. Middle; homogeneous permeability model with $500mD$. Bottom; homogeneous permeability model with $1000md$.

needed to properly resolve the CO_2 plume. The numerical example calculations illustrate important trapping mechanisms. In particular residual gas saturation and stratigraphic traps are considered. The spreading of CO_2 is highly dependent on the relative permeability models that are used. Local domes in

combinations with cap-rock and sealed faults may provide significant practical storage volumes, provided that the integrity of the cap-rocks and faults can be verified. The impact of permeability description has been discussed and is shown to have significant effect on the simulated saturation distributions.

6. Acknowledgments

References

[1] Aavatsmark, I, E. Reiso, R. Teigland (2001), *Control-Volume Discretization Methods for Quadrilateral Grids with Faults and Local Refinement*, Computational Geosciences **5**, pp 1-23.

[2] Aavatsmark, I., E. Reiso, H. Reme, R. Teigland (2001), *MPFA for Faults and Local Grid Refinement in 3D Quadrilateral Grids With Application to Field Simulations*, SPE 66356, Proceedings of SPE Reservoir Simulation Symposium, Houston, Texas.

[3] Aavatsmark, I., G.T. Eigestad, B.-O. Heimsund, B. Mallison, J.M. Nordbotten, E. Øian (2007), *A New Finite Volume Approach to Efficient Discretization on Challenging Grids*, SPE 106435, Proceedings of SPE Reservoir Simulation Symposium, Houston, Texas.

[4] Bachu S. (2008), *CO_2 storage in geological media: Role, means, status and barriers to deployment*, Progress in Energy and Combustion Science, **34**, pp 254-273

[5] Bachu S., D. Bonijoly, J. Bradshaw, R. Burruss, S. Holloway, N.P. Christensen, and O.M. Mathiassen (2007), *CO_2 storage capacity estimation: Methodology and gaps*, Int. Journal on Greenhouse Gas Control, **1**, pp 430-443

[6] Bergmo, P.E, E. Lindeberg, F. Riis, W.T. Johansen (2008), *Exploring geological storage sites for CO_2 for Norwegian gas power plants: Johansen formation*, Proceedings of GHGT-9, 16.-20. November 2008.

[7] Bradshaw J., S. Bachu, D. Bonijoly, R. Burruss, S. Holloway, N.P. Christensen, and O.M. Mathiassen (2007), *CO_2 storage capacity estimation: Issues and development of standards*, Int. Journal on Greenhouse Gas Control, **1**, pp 62-68

[8] Class, H., H. Dahle, F. Riis, A. Ebigbo, and G. Eigestad (2008), *Estimation of the CO_2 Storage Capacity of a Geological, Numerical Investigations of CO_2 Sequestration in Geological Formations: Problem Oriented Benchmarks*, http://www.iws.uni-stuttgart.de/CO2-workshop/

[9] Gassnova (2007), *Beslutningsgrunnlag knyttet til transport og deponering av CO_2 fra Kårstø og Mongstad*, Report no 06/177, (In Norwegian)

[10] Ebigbo A., J.M. Nordbotten, and H. Class (2008), *CO_2 Plume Evolution and Leakage through an Abandoned Well, Numerical Investigations of CO_2 Sequestration in Geological Formations: Problem Oriented Benchmarks*, http://www.iws.uni-stuttgart.de/CO2-workshop/

[11] Eigestad, G.T, H. Dahle, B. Hellevang, W.T. Johansen, K.-A. Lie, F. Riis and E. Øian (2008), *Geological and fluid data for modelling CO2-injection in the Johansen formation*, http://org.uib.no/cipr/Project/MatMoRA/Johansen/index.htm (to be made available)

[12] Sclumberger (2006), Eclipse 100/300 Reference Manual and Technical Manual

[13] Juanes, R., E.J. Spiteri, F.M. Orr Jr., and M. J. Blunt (2006), *Impact of relative permeability hysteresis on geological CO_2 storage*, Wat. Res. Research, **42**

[14] Lindeberg, E., P. Zweigel, P. Bergmo, A. Ghaderi, and A. Lothe (2001), *Prediction of CO_2 distribution pattern improved by geology and reservoir simulations*, Proceedings of the Fifth Int. Conf. on Greenhouse Gas Reduction Technologies

[15] Lindeberg, E., and P. Bergmo (2003), *The long-term fate of CO_2 injected into an aquifer Prediction*, Proceedings of the Sixth Int. Conf. on Greenhouse Gas Reduction Technologies

[16] NIST Chemistry web-book, `http://webbook.nist.gov/chemistry`

[17] Manzocchi, T., J.J. Walsh, P. Nell and G. Yielding (1999), *Fault Transmissibility Multipliers for Flow Simulation Models*, Petroleum Geoscience, **5**, pp 53-63

[18] Nordbotten, J. M. and M. A. Celia (2006), *An improved analytical solution for interface upconing around a well*, Water Resources Research, **42**

[19] Nordbotten, J. M. and M. A. Celia (2006), *Similarity Solutions for Fluid Injection into Confined Aquifers*, Journal of Fluid Mechanics, **561**, pp 307-327

[20] Nordbotten, J. M., M. A. Celia, S. Bachu and H. K. Dahle (2005), *Semi-Analytical Solution for CO_2 Leakage through an Abandoned Well*, Environmental Science and Technology, **39**(2), pp 602-611

[21] Nordbotten, J. M., M. A. Celia and S. Bachu (2005), *Injection and Storage of CO_2 in Deep Saline Aquifers: Analytical Solution for CO_2 Plume Evolution During Injection*, Transport in Porous Media, **58**(3), pp 339-360

[22] Nordbotten, J. M., M.A. Celia and S. Bachu (2004), *Analytical Solutions for Leakage Rates Through Abandoned Wells*, Water Resources Research, **40**

[23] Schlumberger (2007), Petrel Reference Manual

[24] Torp, T.A., JJ. Gale (2004), *Demonstrating storage of the CO_2 in geological reservoirs: The Sleipner and SACS projects*, Energy **29**, pp 1361-1369

[25] Ponting, D.K. (1992), *Corner Point Geometry in Reservoir Simulation*, Proceedings of the 1st European Conference on the Mathematics of Oil Recovery, Cambridge, Clarendon Press, Oxford, pp 45-65.

[26] Pruess, K., T. Xu, J. Apps, J. Garcia (2003), *Numerical Modeling of Aquifer Disposal of CO_2*, SPE **8** (1), pp. 49-60.

(Geir Terje Eigestad) DEP. OF MATHEMATICS, UNIVERSITY OF BERGEN/
PERECON AS, BERGEN, NORWAY
E-mail address: `geirte@math.uib.no`

(Helge K. Dahle) DEP. OF MATHEMATICS,
UNIVERSITY OF BERGEN, NORWAY
E-mail address: `helge.dahle@math.uib.no`

(Bjarte Hellevang) RESLAB INTEGRATION,
BERGEN, NORWAY
E-mail address: `bjarte.hellevang@ri.reslab.no`

(Fridtjof Riis) NORWEGIAN PETROLEUM DIRECTORATE,
STAVANGER, NORWAY
E-mail address: `Fridjof.Riis@iris.no`

(Wenche Tjelta Johansen) NORWEGIAN PETROLEUM DIRECTORATE,
STAVANGER, NORWAY
E-mail address: `Wenche.Johansen@npd.no`

(Erlend Øian) PERECON AS,
BERGEN, NORWAY
E-mail address: `erlend.oian@perecon.no`